

Accelerated glacier mass loss in the Southeast Tibetan Plateau is dominated by phase change of monsoon precipitation

A. Jouberton¹, T. E. Shaw¹, E. Miles¹, M. McCarthy^{1,5}, S. Fugger^{1,6}, A. Dehecq⁷, S. Ren^{1,2}, W. Yang^{3,4}, C. Zhao³, F. Pellicciotti^{1,8}

¹Swiss Federal Institute for Forest, Snow and Landscape Research (WSL), Birmensdorf, Switzerland

²State Key Laboratory of Remote Sensing Science, Aerospace Information Research Institute, Chinese Academy of Sciences, Beijing 100101, China

³Institute of Tibetan Plateau Research, Chinese Academy of Sciences, Beijing, China

⁴Ministry of Education Key Laboratory for Earth System Modelling, Department of Earth System Science, Tsinghua University, Beijing, China

⁵British Antarctic Survey, Natural Environment Research Council, Cambridge, UK

⁶Institute of Environmental Engineering, ETH Zurich, 8093 Zurich, Switzerland

⁷Laboratory of Hydraulics, Hydrology and Glaciology (VAW), ETH Zurich, 8093, Zurich, Switzerland

⁸Department of Geography, Northumbria University, Newcastle, UK

 interactive

Introduction

Study site

Methods

Results

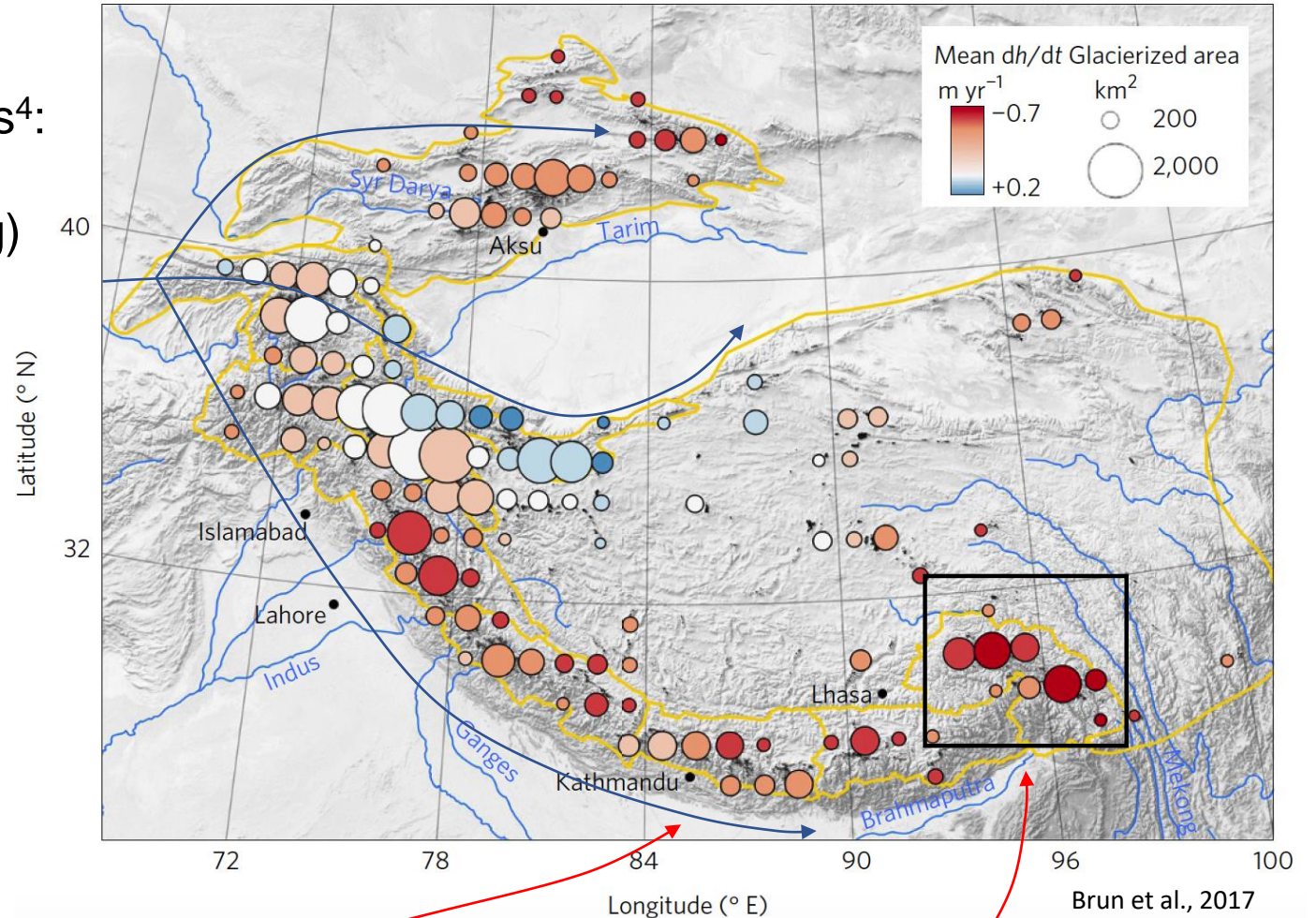
Discussion

References

Supplementary

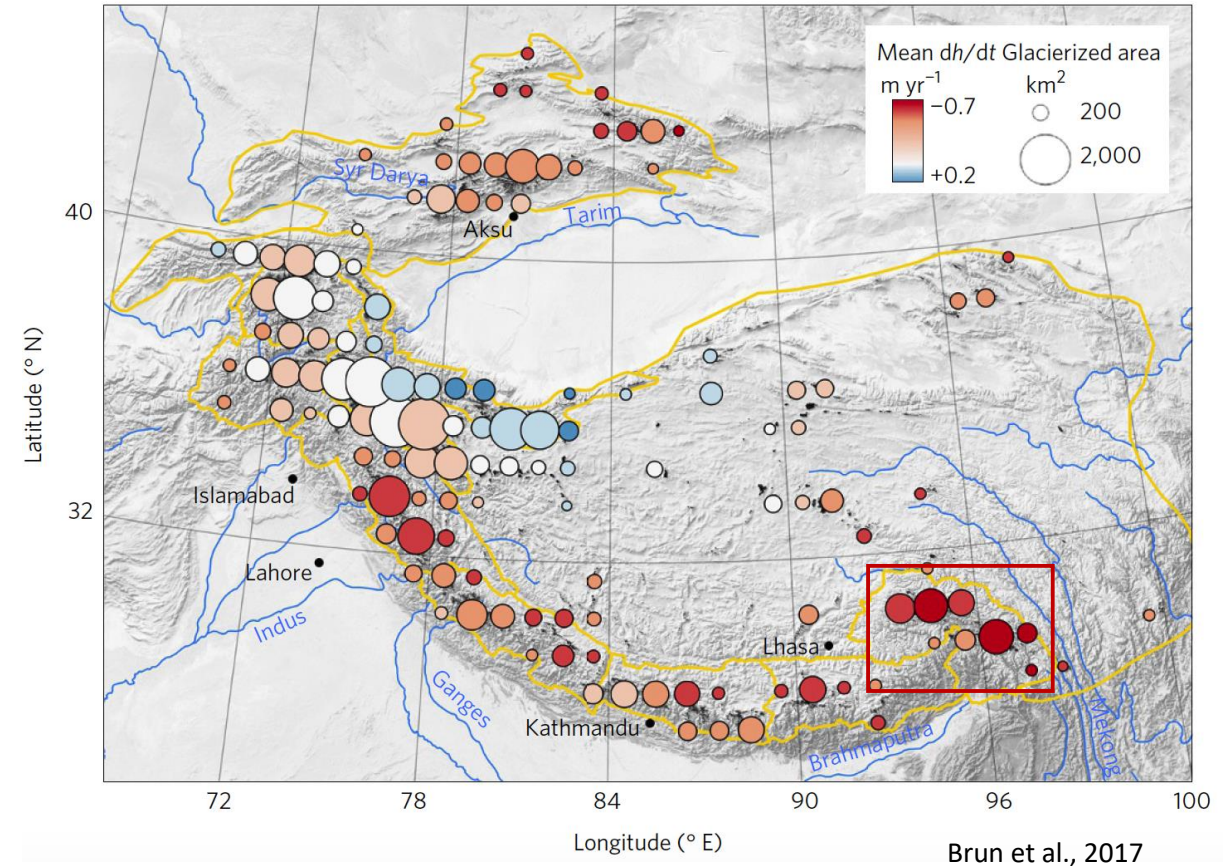
- Mountains are the water towers of Asia¹, and glaciers experienced widespread shrinking due to global warming over the last decades^{2,3}
- Two global atmospheric circulation patterns⁴:
 - Westerlies (mostly in winter and spring)
 - Indian monsoon (in summer)
- Highest glacier mass losses observed in southeast Tibetan Plateau^{2,4,5}
- Mass loss accelerated over the last 4 decades⁶

Indian monsoon
 Westerlies



Research questions :

- What are the drivers and processes explaining this mass loss acceleration ?
- What are the implications for catchment runoff ?



Parlung No. 4 Glacier

Classification: maritime⁷, spring-accumulation^{8,9}, debris-free, valley-type.

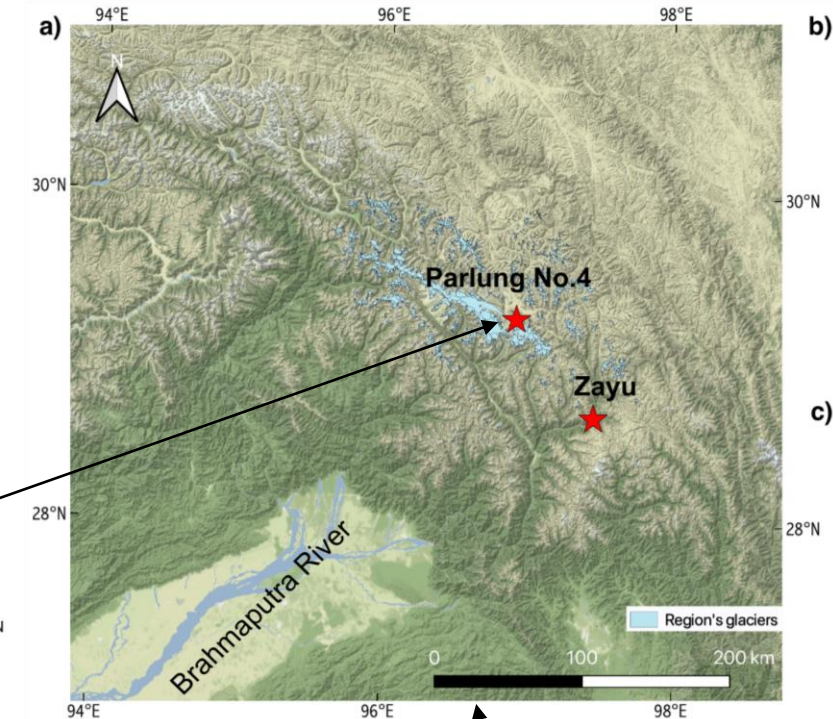
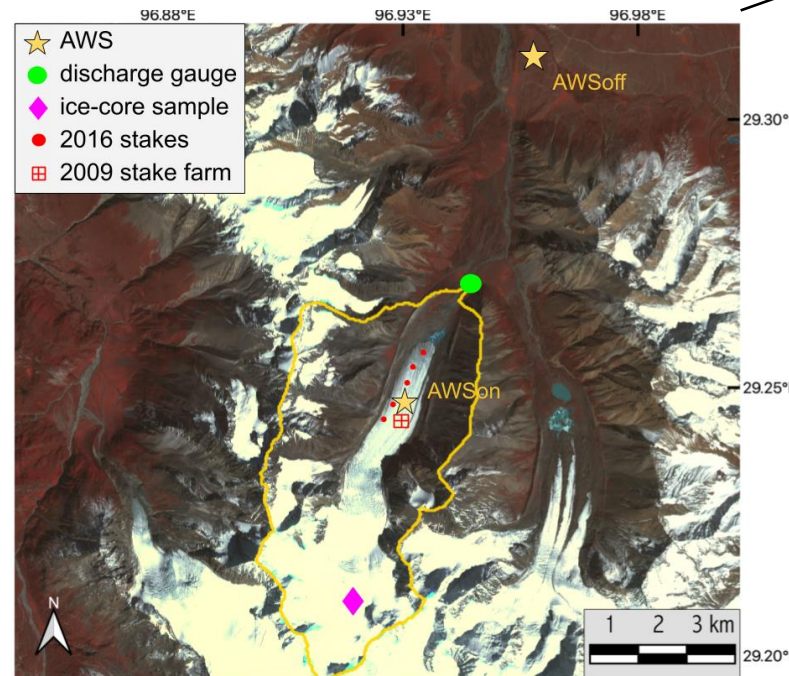
Elevation range: 4650 to 5964 m a.s.l.

Glacier area and length: 11.7 km² and 8 km

Coordinates: 29°14', 96°56'E

Catchment area: 24.4 km²

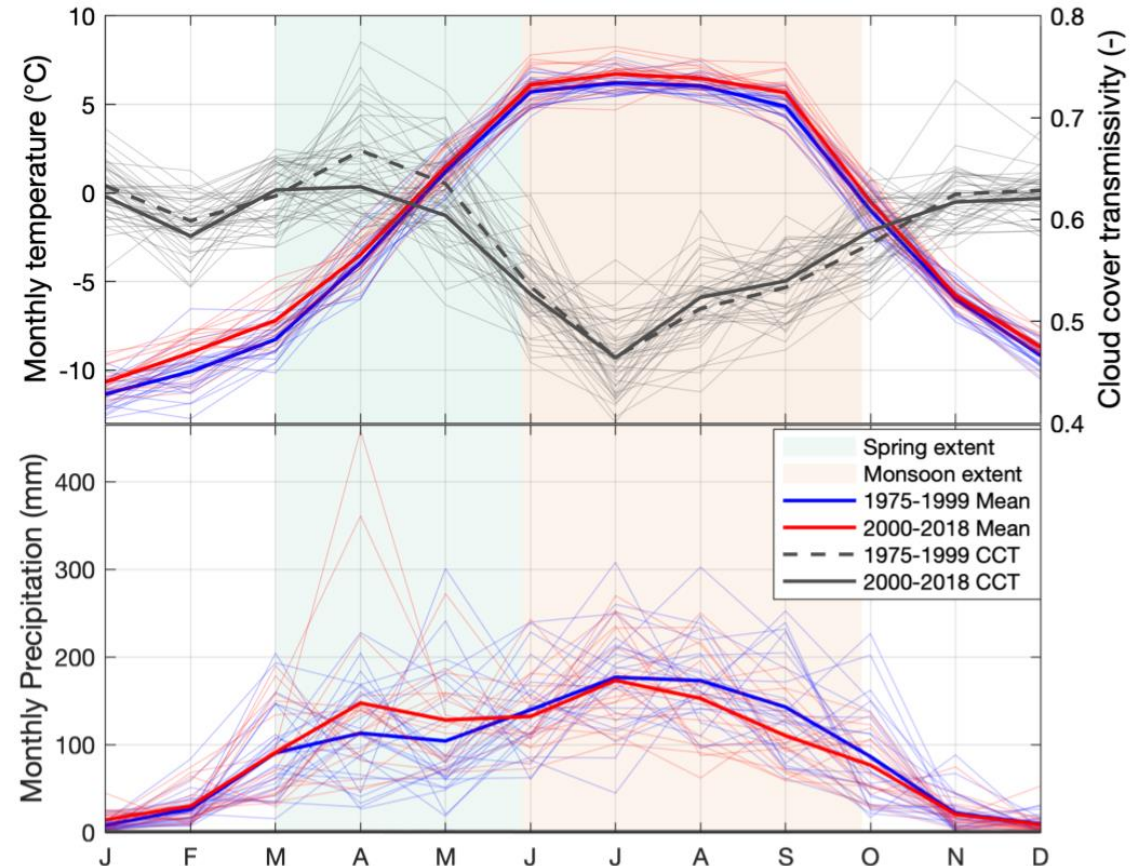
- Considered as a benchmark glacier in this region, since its meteorology, surface energy fluxes and mass-balance have each been examined in recent years^{10,11,12}.



Parlung No. 4 Glacier

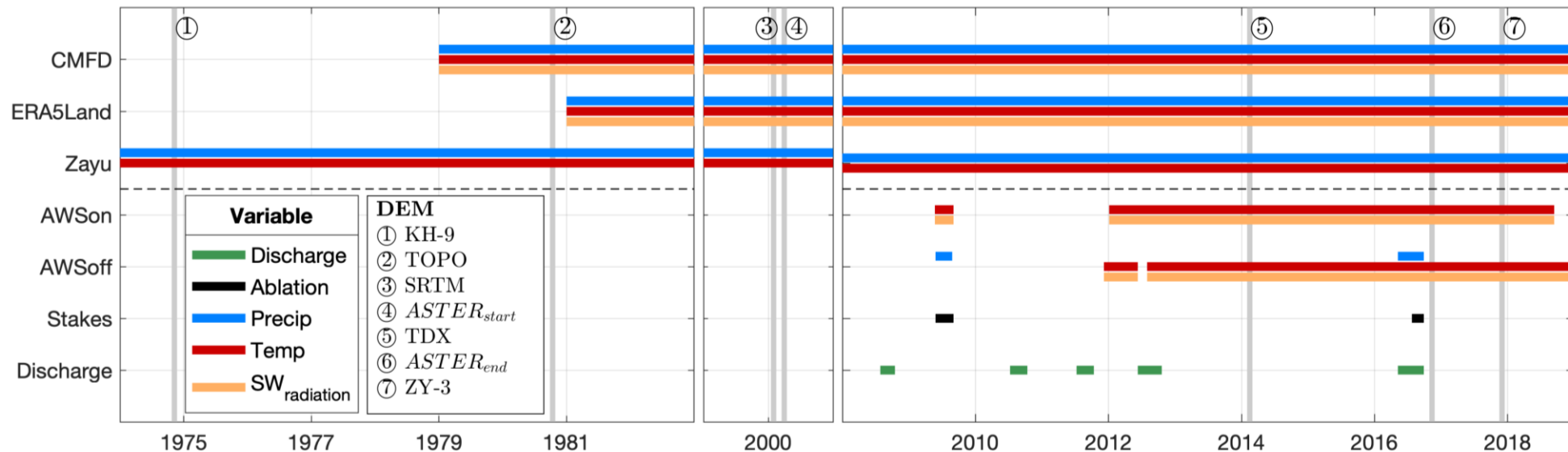
Climate of the region :

- Influenced by southern westerlies and the Bay of Bengal vortex during spring, and by the Indian monsoon in summer.
- One of the wettest places in the Tibetan Plateau, with annual sum amounting to 1000-3000 mm⁷.
- Double-peak precipitation pattern, with around 30% and 44% of annual precipitation falling in spring (Mar-May) and summer (Jun-Aug) respectively.



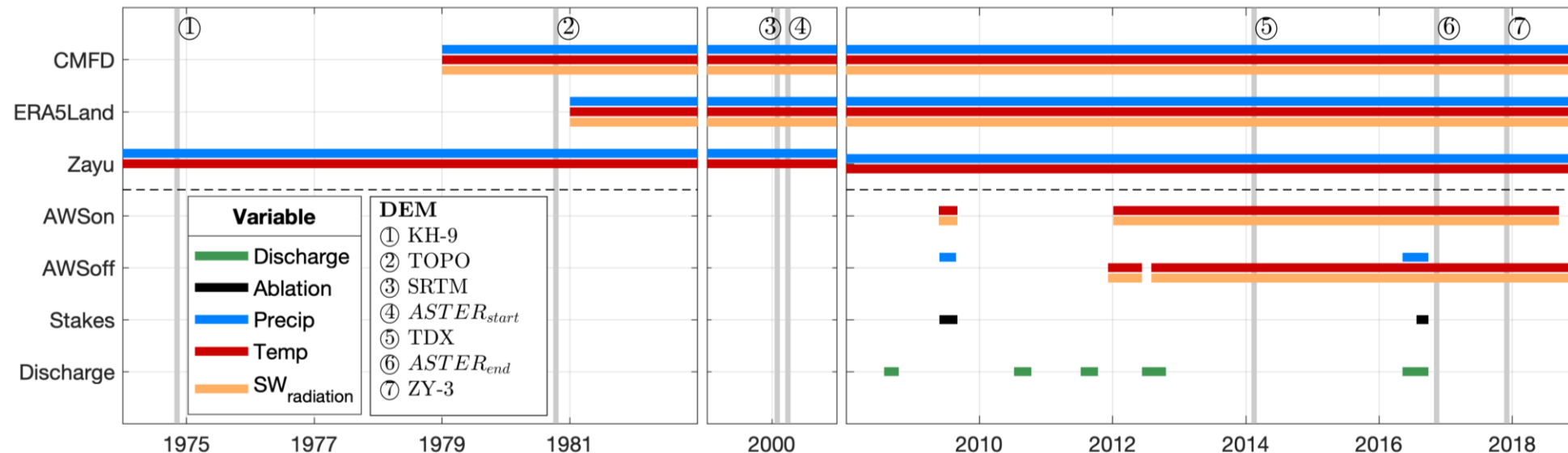
Data availability

- Meteorological forcing : off-glacier AWS, national weather station at Zayu, reanalysis datasets (CMFD¹³ and ERA5-Land¹⁴).
- In-situ observation : discharge, ablation stakes, ice-core drill sample, surface energy fluxes.
- Remote-sensing observation: Digital elevation models, elevation change maps for different periods, MODIS fractional snow cover.



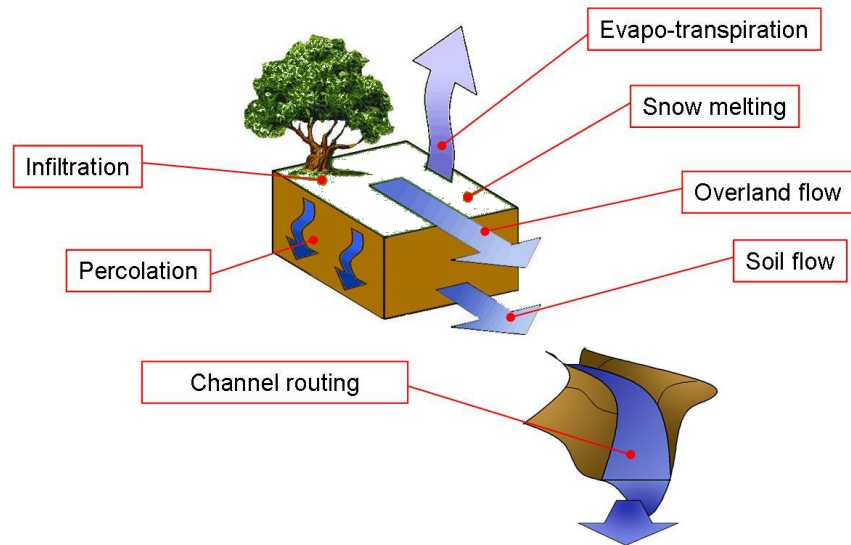
Meteorological forcing reconstruction

- Only few years of in-situ meteorological measurements, but need for 45 years of continuous forcing to run the model.
- Bias-correction of reanalysis datasets (CMFD and ERA5-Land) and Zayu's weather station data with AWS data, selection of the best performing dataset.



Glacio-hydrological model : TOPKAPI-ETH

- fully distributed
- process oriented



- 30m spatial resolution
- hourly time step
- run from 1975 to 2019

Ice and snow melt: Enhanced ETI model

$$M = \begin{cases} TF \cdot T_i + SRF \cdot (1 - \alpha_i) \cdot I_{\downarrow i} & T_i > T_T \\ 0 & T_i \leq T_T \end{cases} \quad \text{Pellicciotti et al. (2005)}^{22}$$

Albedo parameterization :

$$\alpha = \begin{cases} \alpha_{Snow_i} & SNOW_{Depth} > 0 \\ \alpha_{Ground_i} & SNOW_{Depth} = 0 \text{ and cell } i \text{ not glacierized} \\ \alpha_{Ice_i} & SNOW_{Depth} = 0 \text{ and cell } i \text{ glacierized} \end{cases}$$

Brock et al. (2000)²³

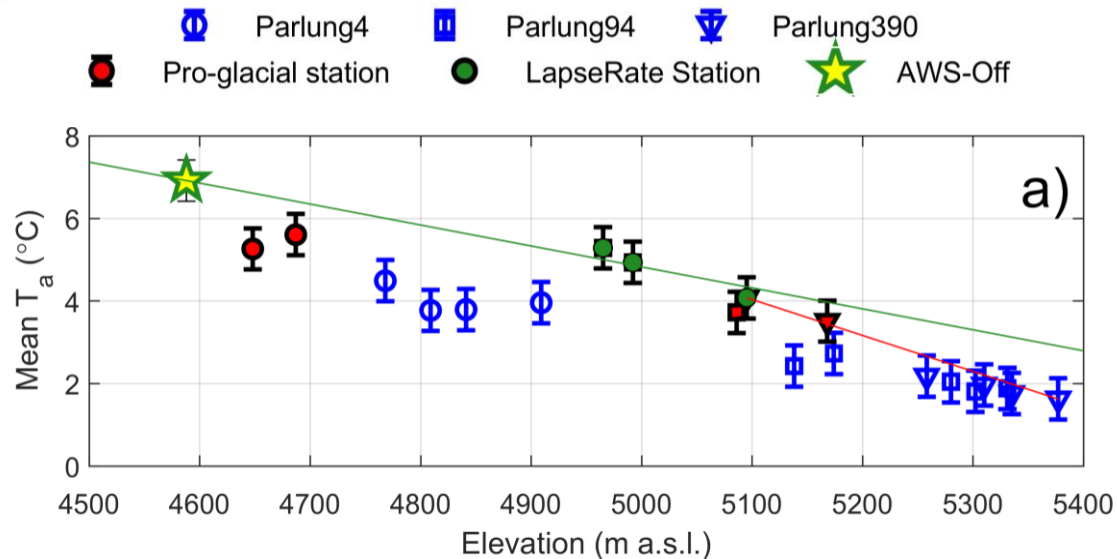
$$\alpha_{snow_i} = Alb f_1 + Alb f_2 \cdot \log_{10}(T_{acc_i})$$



Calibrated using on-glacier AWS data

Meteorological forcing distribution

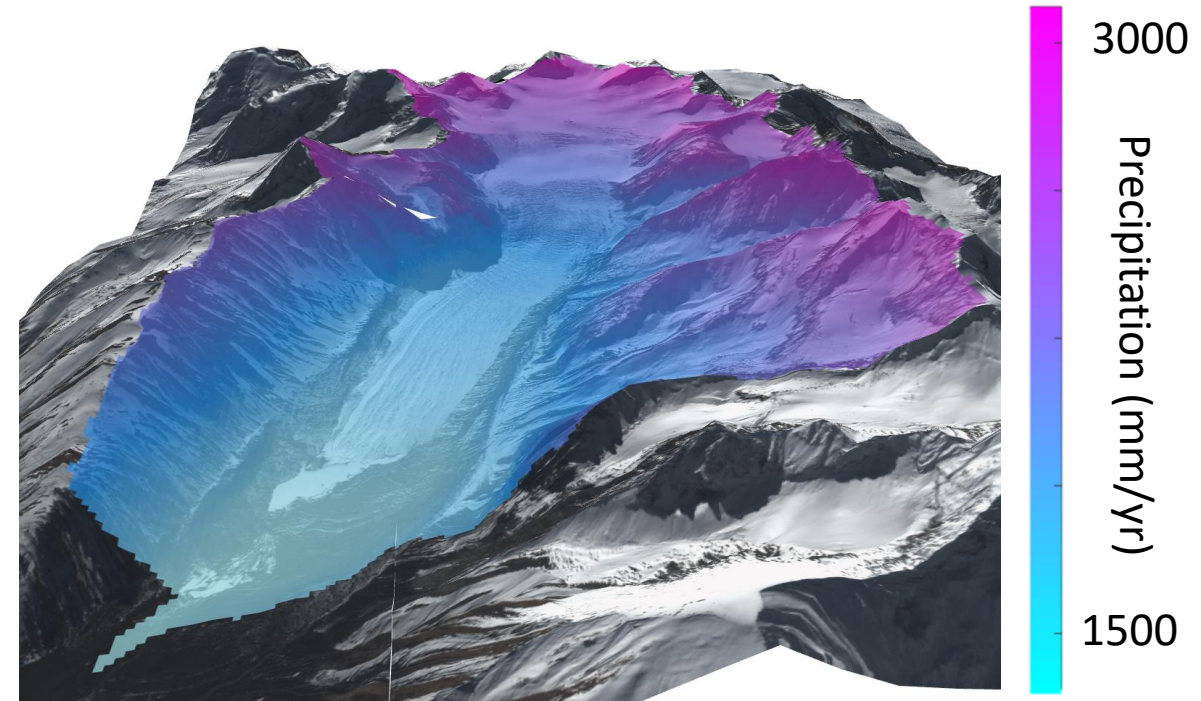
Temperature extrapolation



Shaw et al. (2021)²⁴

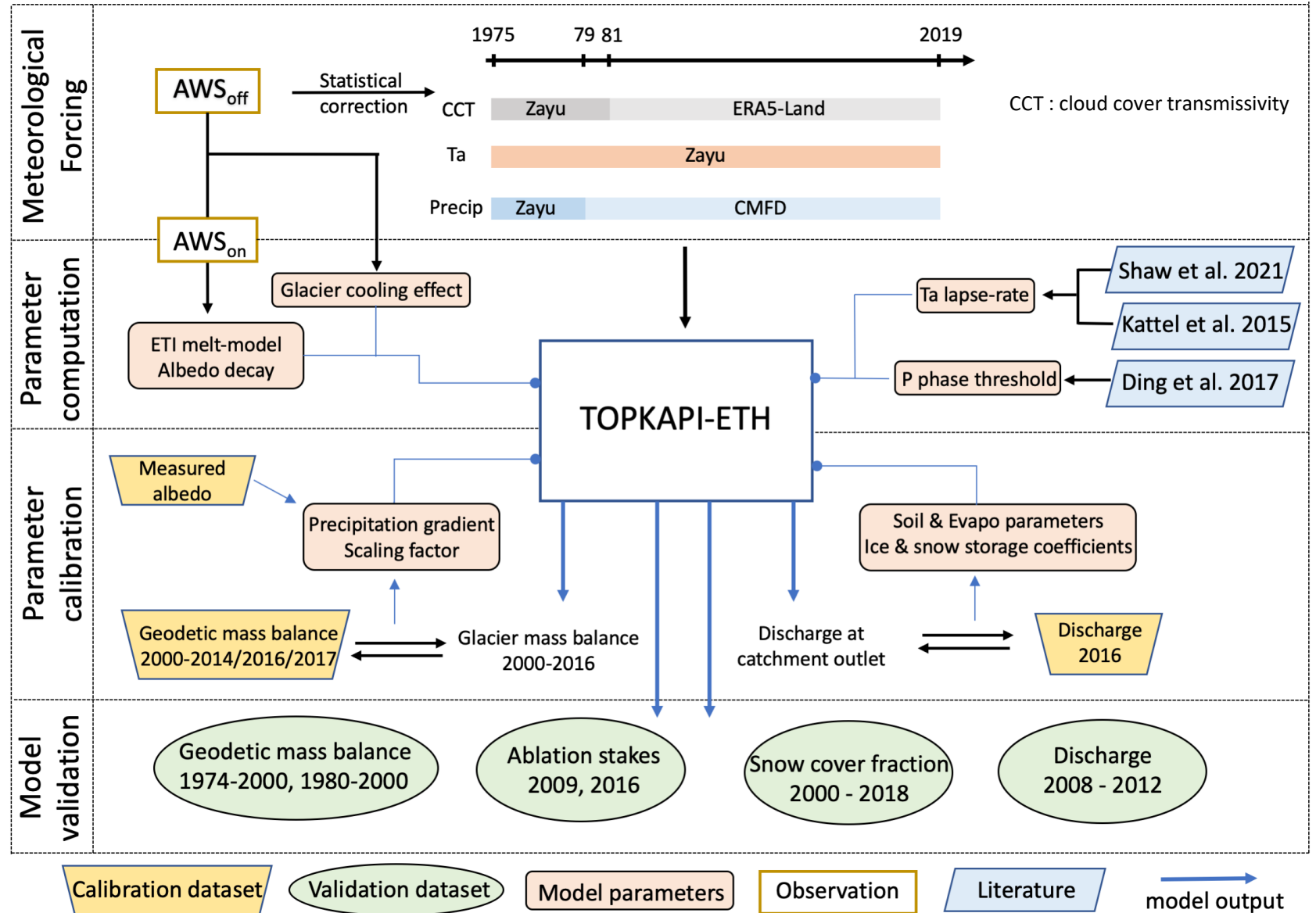
Mean lapse-rates and glacier cooling effect derived from T-loggers installed during a 2018-2019 campaign

Precipitation extrapolation



Precipitation gradient calibrated against geodetic mass balance and measured albedo

Model set-up procedure summary



Catchment solid water balance

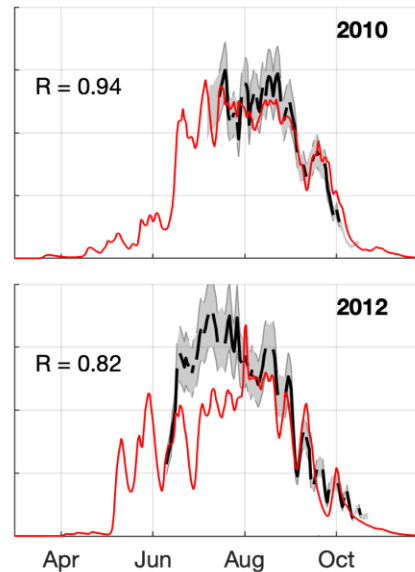
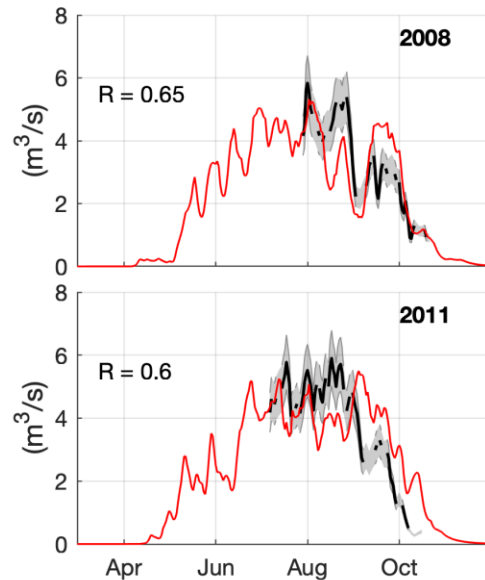
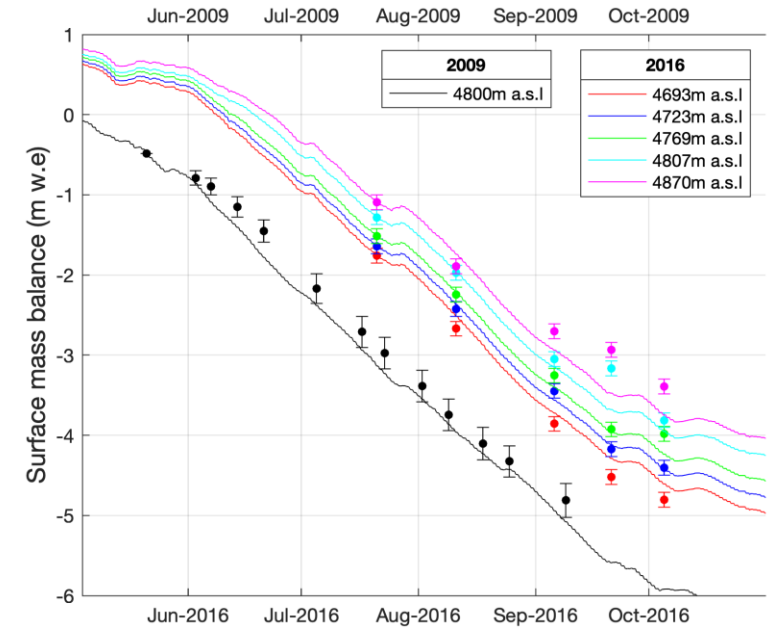
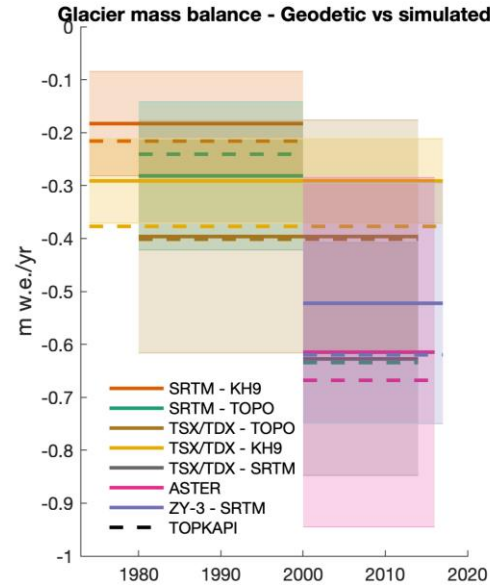
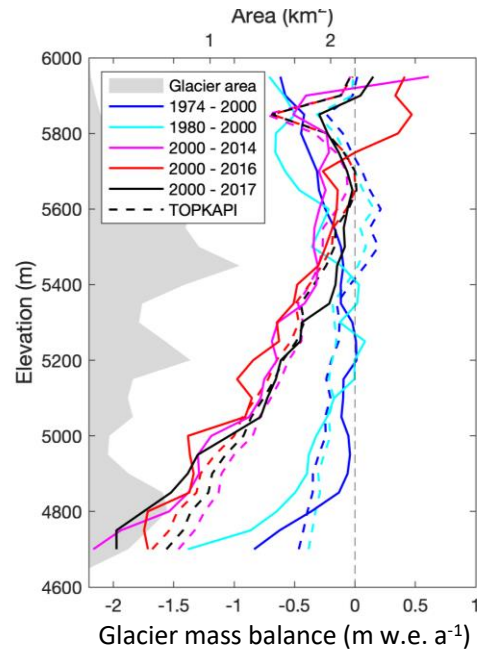
- Catchment solid water storage: water stored as ice or snow in the catchment.
- Catchment solid water balance :

$$\Delta_{\text{storage}} = \text{Solid precipitation} - \text{Icemelt} - \text{Snowmelt}$$

- We quantify the relative contribution of each component to cause the additional glacier mass loss of the recent period (2000-2018).
- A change in solid precipitation can be due to :
 - a change in precipitation amount
 - a change in the rain-snowfall ratio

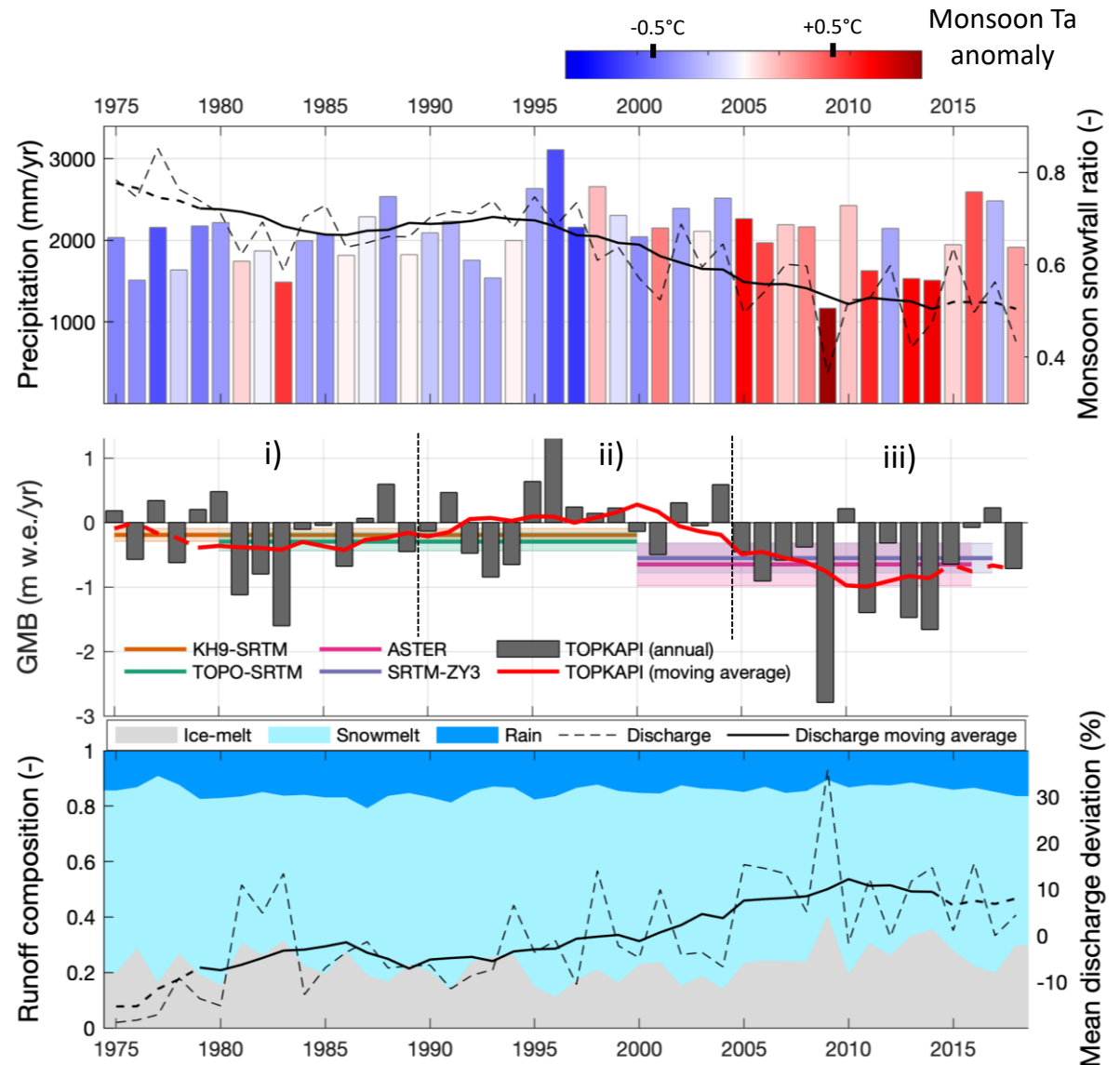
Model performance

- Good match with ablation stakes and measured discharge.
- Reproduces well the geodetic mass balance of the different sub-periods.



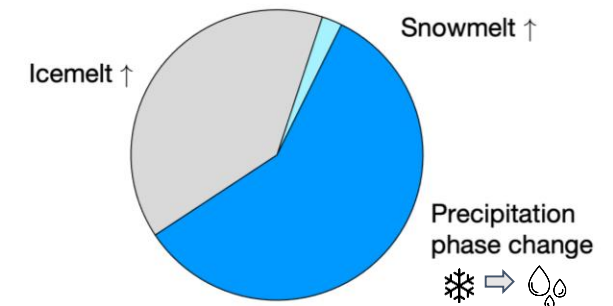
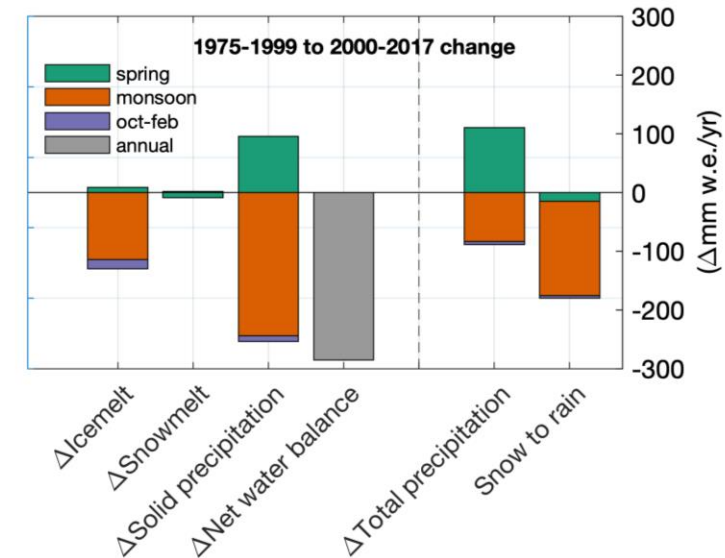
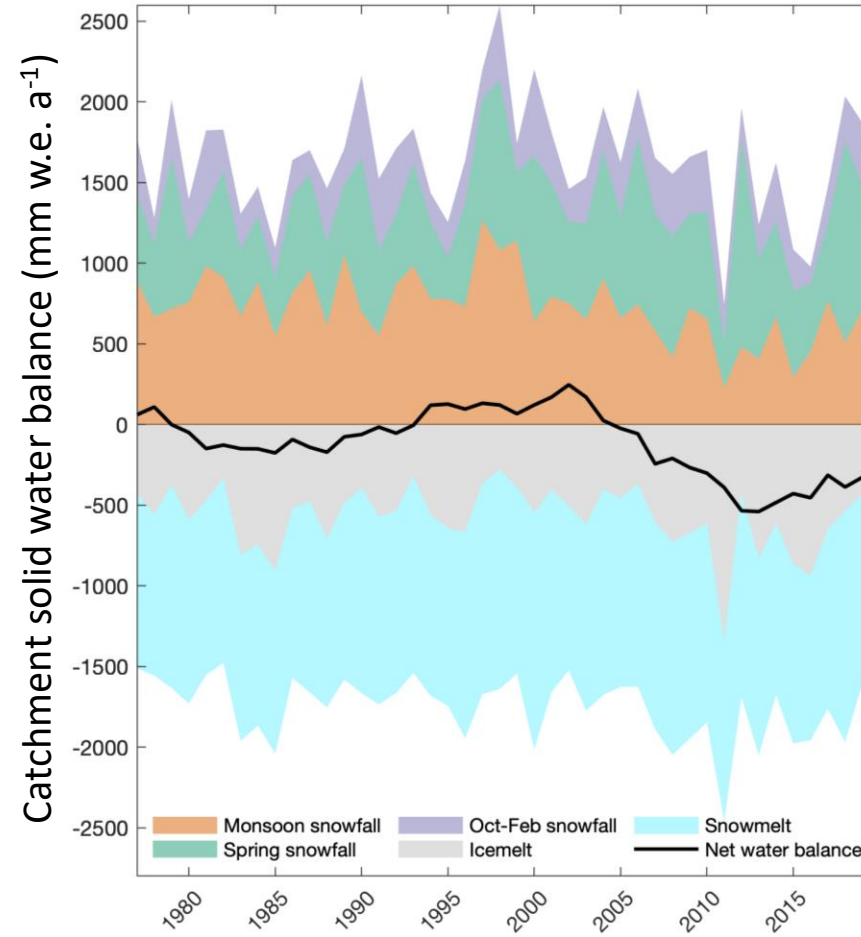
Reconstruction of climatic forcing and catchment hydrology since 1975

- Three distinct periods of glacier-mass balance :
 - i) $-0.28 \text{ m w.e. a}^{-1}$ in 1975-1989
 - ii) $+0.07 \text{ m w.e. a}^{-1}$ in 1990-2004
 - iii) $-0.78 \text{ m w.e. a}^{-1}$ in 2005-2018
- Significant warming of $0.39^{\circ}\text{C .dec}^{-1}$ since the 1990s.
- Increase in catchment runoff of 13% between the two geodetic observation periods (1975-1999 and 2000-2018), mostly driven by a 23% increase in ice-melt.



Drivers of recent glacio-hydrological changes

- From 1975-1999 to 2000-2018, the recent additional mass loss was due to less annual snowfall (-158 mm) and more snow- and ice-melt (+7 and +121 mm).
- Seasonal changes are more contrasted: solid precipitation increased in spring (+ 96 mm) but decreased sharply in monsoon months (- 244 mm).
- Monsoon snowfall decrease mostly caused by precipitation phase change, as well as a decrease in precipitation amounts.



Implications

- The role of precipitation phase change in explaining those glaciers' sensitivity to temperature change was suggested in previous studies^{15,16} through sensitivity analyses. Here we attribute the recent mass loss to this change in precipitation phase during the monsoon months (Jun-Sep), and to the concurrent ice-melt intensification.
- Spring precipitation phase is still largely unaffected by the warming, thus spring accumulation became increasingly important in providing mass to the glacier.
- Decadal changes in precipitation can compensate for or accentuate the warming-induced losses, but even the observed slight increase in spring precipitation was unable to slow the rapid decline of glaciers in the southeast TP.
- The catchment discharge increase due to enhanced ice-melt could raise the risk of glacier lake outburst flood occurrence in a region which is already classified as high hazard zone¹⁷.

Future work

- This model set-up could be used for future projection to estimate when the maximum contribution of glacier melt to catchment runoff is likely to occur (peak water).
- The understanding of the complex interactions between spring and monsoon precipitation and their decadal changes could be improved by using a new suite of high resolution atmospheric models that reduce uncertainty in spatially-resolved, convective precipitation and meteorological forcing^{18,19}.
- Future predictions could be improved by more utilizing physically-based, land-surface models which incorporate detailed parameterizations of phase change thresholds¹¹ and account for meltwater refreezing²⁰ as well as sublimation²¹ and snow redistribution.

Reference

- [1] Immerzeel, W. W., Van Beek, L. P. H., & Bierkens, M. F. P. (2010). Climate change will affect the Asian water towers. *Science*, 328(5984), 1382–1385. <https://doi.org/10.1126/science.1183188>
- [2] Brun, F., Berthier, E., Wagnon, P., Käab, A., & Treichler, D. (2017). A spatially resolved estimate of High Mountain Asia glacier mass balances from 2000 to 2016. *Nature Geoscience*, 10(9), 668–673. <https://doi.org/10.1038/ngeo2999>
- [3] Bolch, T., Shea, J. M., Liu, S., Azam, F. M., Gao, Y., Gruber, S., ... Zhang, Y. (2019). Status and Change of the Cryosphere in the Extended Hindu Kush Himalaya Region. In *The Hindu Kush Himalaya Assessment* (pp. 209–255). Springer International Publishing. https://doi.org/10.1007/978-3-319-92288-1_7
- [4] Yao, T., Thompson, L., Yang, W., Yu, W., Gao, Y., Guo, X., ... Joswiak, D. (2012). Different glacier status with atmospheric circulations in Tibetan Plateau and surroundings. *Nature Climate Change*, 2(9), 663–667. <https://doi.org/10.1038/nclimate1580>
- [5] Shean, D. E., Bhushan, S., Montesano, P., Rounce, D. R., Arendt, A., & Osmanoglu, B. (2020). A Systematic, Regional Assessment of High Mountain Asia Glacier Mass Balance. *Frontiers in Earth Science*, 7, 363. <https://doi.org/10.3389/feart.2019.00363>
- [6] Wu, K., Liu, S., Jiang, Z., Xu, J., Wei, J., & Guo, W. (2018). Recent glacier mass balance and area changes in the Kangri Karpo Mountains from DEMs and glacier inventories. *Cryosphere*, 12(1), 103–121. <https://doi.org/10.5194/tc-12-103-2018>
- [7] Shi, Y., & Liu, S. (2000). Estimation on the response of glaciers in China to the global warming in the 21st century. *Chinese Science Bulletin*, 45(7), 668–672. <https://doi.org/10.1007/BF02886048>
- [8] Yang, W., Yao, T., Guo, X., Zhu, M., Li, S., & Kattel, D. B. (2013). Mass balance of a maritime glacier on the southeast Tibetan Plateau and its climatic sensitivity. *Journal of Geophysical Research Atmospheres*, 118(17), 9579–9594. <https://doi.org/10.1002/jgrd.50760>
- [9] Maussion, F., Scherer, D., Mölg, T., Collier, E., Curio, J., & Finkelnburg, R. (2014). Precipitation seasonality and variability over the Tibetan Plateau as resolved by the high Asia reanalysis. *Journal of Climate*, 27(5), 1910–1927. <https://doi.org/10.1175/JCLI-D-13-00282.1>
- [10] Yang, W., Guo, X., Yao, T., Yang, K., Zhao, L., Li, S., & Zhu, M. (2011). Summertime surface energy budget and ablation modeling in the ablation zone of a maritime Tibetan glacier. *Journal of Geophysical Research Atmospheres*, 116(14). <https://doi.org/10.1029/2010JD015183>
- [11] Ding, B., Yang, K., Yang, W., He, X., Chen, Y., Lazhu, ... Yao, T. (2017). Development of a Water and Enthalpy Budget-based Glacier mass balance Model (WEB-GM) and its preliminary validation. *Water Resources Research*, 53(4), 3146–3178. <https://doi.org/10.1002/2016WR018865>
- [12] Yang, W., Zhao, C., Westoby, M., Yao, T., Wang, Y., Pellicciotti, F., ... Miles, E. (2020). Seasonal dynamics of a temperate Tibetan glacier revealed by high-resolution UAV photogrammetry and in situ measurements. *Remote Sensing*, 12(15). <https://doi.org/10.3390/RS12152389>
- [13] He, J., Yang, K., Tang, W., Lu, H., Qin, J., Chen, Y., & Li, X. (2020). The first high-resolution meteorological forcing dataset for land process studies over China. *Scientific Data*, 7(1), 1–11. <https://doi.org/10.1038/s41597-020-0369-y>

Reference

- [14] Muñoz-Sabater, J., Dutra, E., Agustí-Panareda, A., Albergel, C., Arduini, G., ..., Thépaut, J.-N.: ERA5-Land: A state-of-the-art global reanalysis dataset for land applications, *Earth Syst. Sci. Data Discuss.* [preprint], <https://doi.org/10.5194/essd-2021-82>, in review, 2021.
- [15] Zhu, M., Yao, T., Yang, W., Xu, B., Wu, G., & Wang, X. (2018). Differences in mass balance behavior for three glaciers from different climatic regions on the Tibetan Plateau. *Climate Dynamics*, 50(9–10), 3457–3484. <https://doi.org/10.1007/s00382-017-3817-4>
- [16] Wang, R., Liu, S., Shangguan, D., Radić, V., & Zhang, Y. (2019). Spatial heterogeneity in glacier mass-balance sensitivity across High Mountain Asia. *Water (Switzerland)*, 11(4). <https://doi.org/10.3390/w11040776>
- [17] Allen, S. K., Zhang, G., Wang, W., Yao, T., & Bolch, T. (2019). Potentially dangerous glacial lakes across the Tibetan Plateau revealed using a large-scale automated assessment approach. *Science Bulletin*, 64(7), 435–445. <https://doi.org/10.1016/j.scib.2019.03.011>
- [18] Collier, E., & Immerzeel, W. W. (2015). High-resolution modeling of atmospheric dynamics in the Nepalese Himalaya. *Journal of Geophysical Research: Atmospheres*, 120(19), 9882–9896. <https://doi.org/10.1002/2015JD023266>
- [19] Bonekamp, P. N. J., Collier, E., & Immerzeel, W. (2018). The Impact of spatial resolution, land use, and spinup time on resolving spatial precipitation patterns in the Himalayas. *Journal of Hydrometeorology*, 19(10), 1565–1581. <https://doi.org/10.1175/JHM-D-17-0212.1>
- [20] Stigter, E. E., Steiner, J. F., Koch, I., Saloranta, T. M., Kirkham, J. D., & Immerzeel, W. W. (2021). Energy and mass balance dynamics of the seasonal snowpack at two high-altitude sites in the Himalaya. *Cold Regions Science and Technology*, 183, 103233. <https://doi.org/10.1016/j.coldregions.2021.103233>
- [21] Ayala, A., Pellicciotti, F., MacDonell, S., McPhee, J., & Burlando, P. (2017). Patterns of glacier ablation across North-Central Chile: Identifying the limits of empirical melt models under sublimation-favorable conditions. *Water Resources Research*, 53(7), 5601–5625. <https://doi.org/10.1002/2016WR020126>
- [22] Pellicciotti, F., Brock, B., Strasser, U., Burlando, P., Funk, M., & Corripio, J. (2005). An enhanced temperature-index glacier melt model including the shortwave radiation balance: Development and testing for Haut Glacier d’Arolla, Switzerland. *Journal of Glaciology*, 51(175), 573–587. <https://doi.org/10.3189/172756505781829124>
- [23] Brock, B. W., Willis, I. C., & Sharp, M. J. (2000). Measurement and parameterization of albedo variations at haut glacier d’arolla, Switzerland. *Journal of Glaciology*, 46(155), 675–688. <https://doi.org/10.3189/172756500781832675>
- [24] Shaw, T. E., Yang, W., Ayala, Á., Bravo, C., Zhao, C., & Pellicciotti, F. (2021). Distributed summer air temperatures across mountain glaciers in the south-east Tibetan Plateau: Temperature sensitivity and comparison with existing glacier datasets. *Cryosphere*, 15(2), 595–614. <https://doi.org/10.5194/tc-15-595-2021>
- [25] Dehecq, A., Gardner, A. S., Alexandrov, O., McMichael, S., Hugonnet, R., Shean, D., & Marty, M. (2020). Automated Processing of Declassified KH-9 Hexagon Satellite Images for Global Elevation Change Analysis Since the 1970s. *Frontiers in Earth Science*, 8. <https://doi.org/10.3389/feart.2020.566802>

Air temperature reconstruction

Precipitation reconstruction

Forcing annual trends

Surface elevation change

Catchment hypsometry

DEM and ice-thickness

Spatial snowfall changes

Discharge seasonality changes

Model performance sensitivity

Results sensitivity

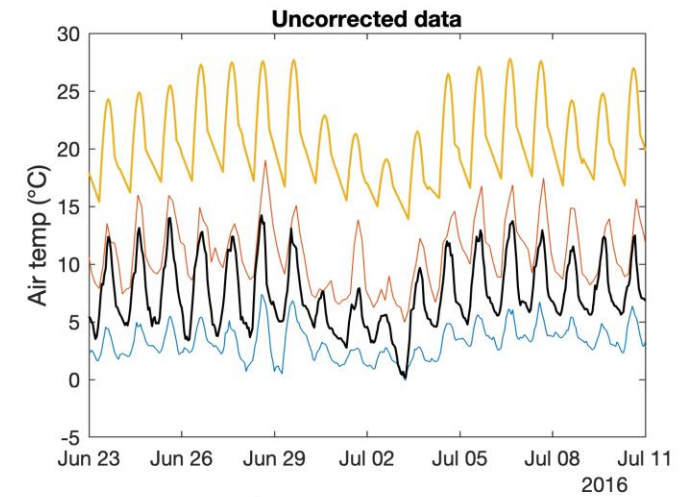
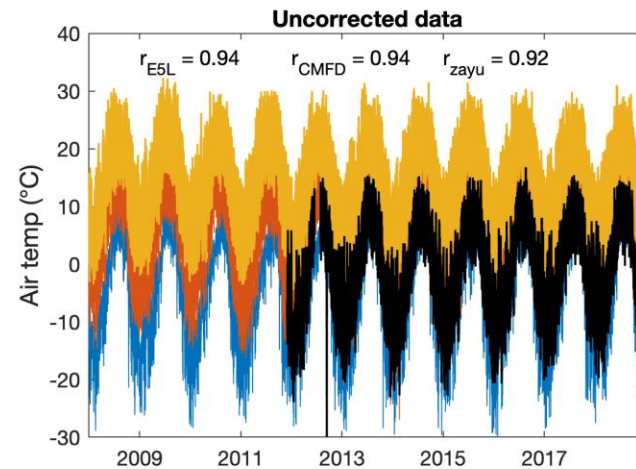
Forcing experiment



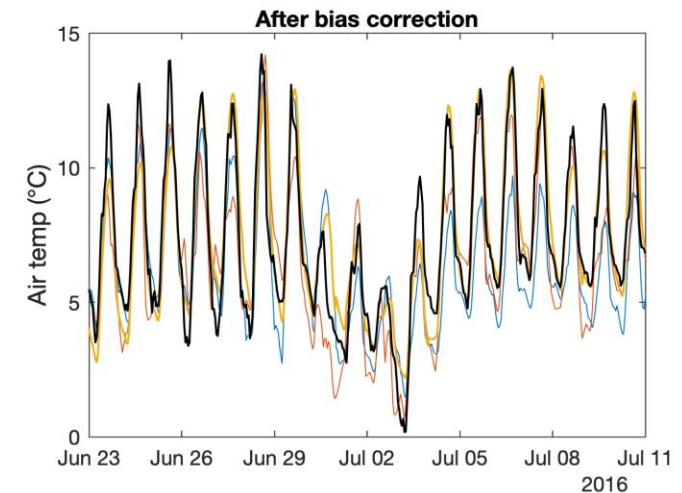
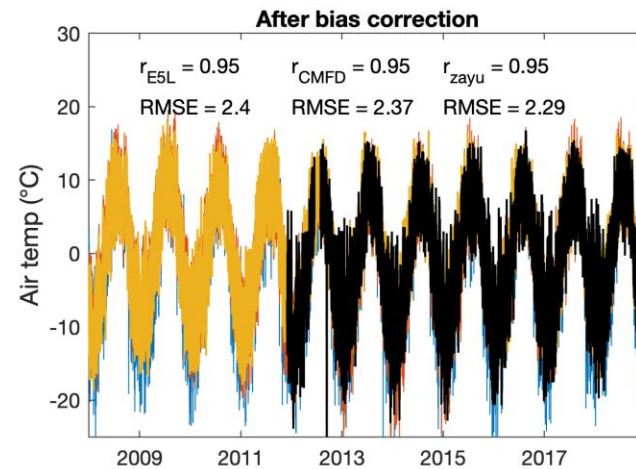
interactive

Air temperature reconstruction

Air temperature comparison between the different data sources, before and after applying a monthly-hourly shift to statistically bias-correct (extrapolate) the reanalysis product (national station data) at the AWS_{off} location.

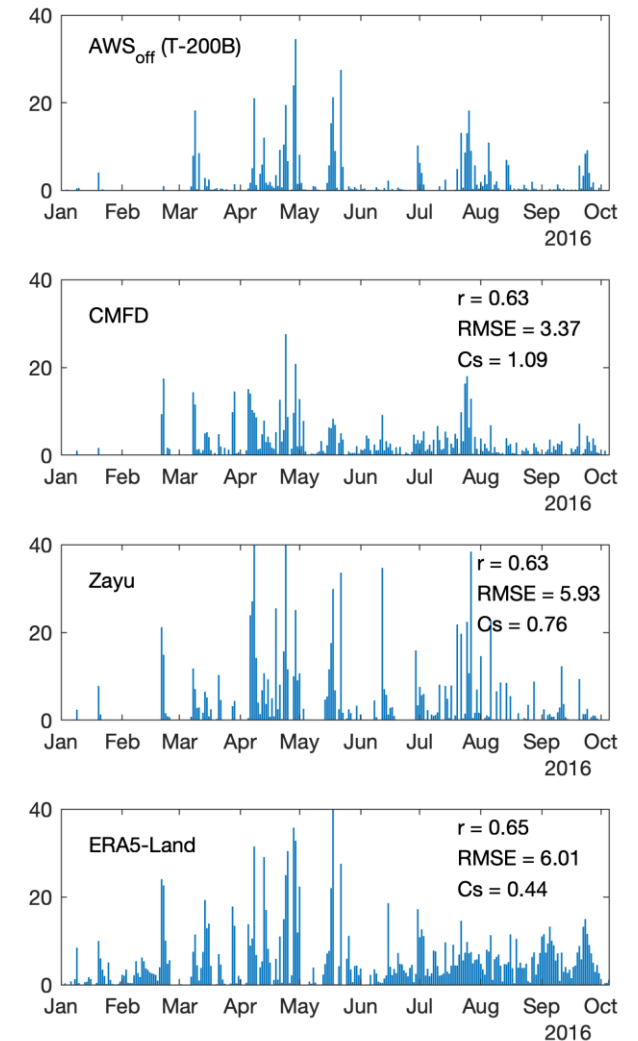
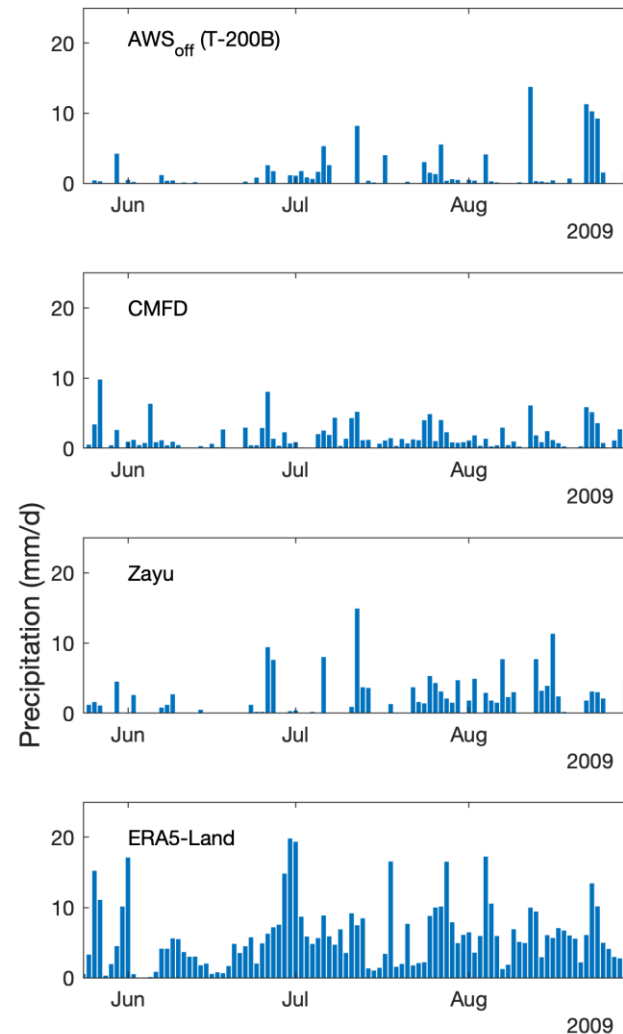


— ERA5Land — CMFD — Zayu — AWSoff



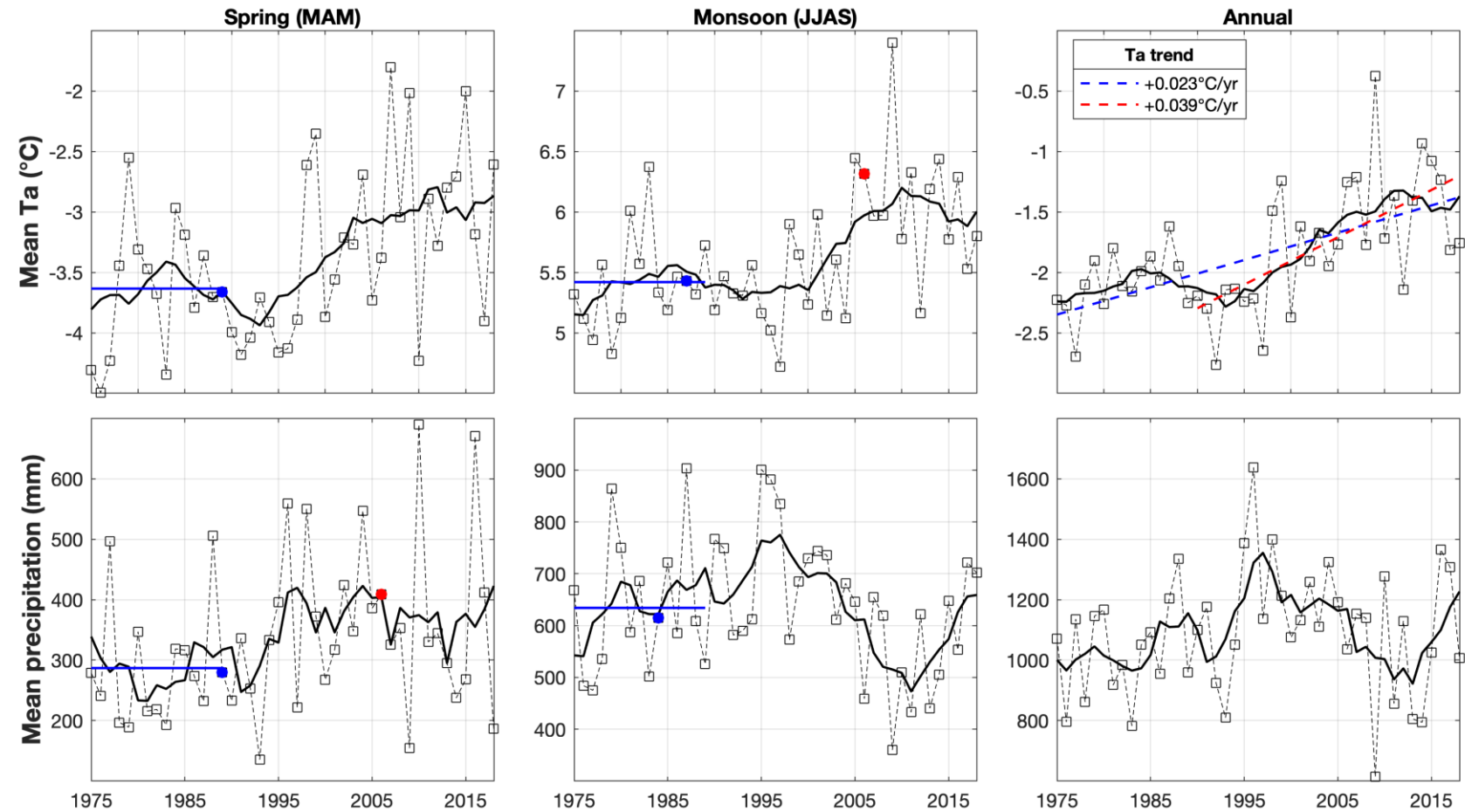
Precipitation reconstruction

Daily precipitation comparison between the different data sources. The Pearson correlation coefficient (r) and root-mean-square error (RMSE) are computed between the precipitation measured at AWS_{off} (T-200B) and the precipitation from the source (CMFD, Zayu or ERA5-Land) mentioned in the corresponding subplot. The precipitation scaling factor (C_s) is computed as the ratio of total precipitation amounts measured at AWS_{off} and total precipitation amounts obtained for the corresponding source.



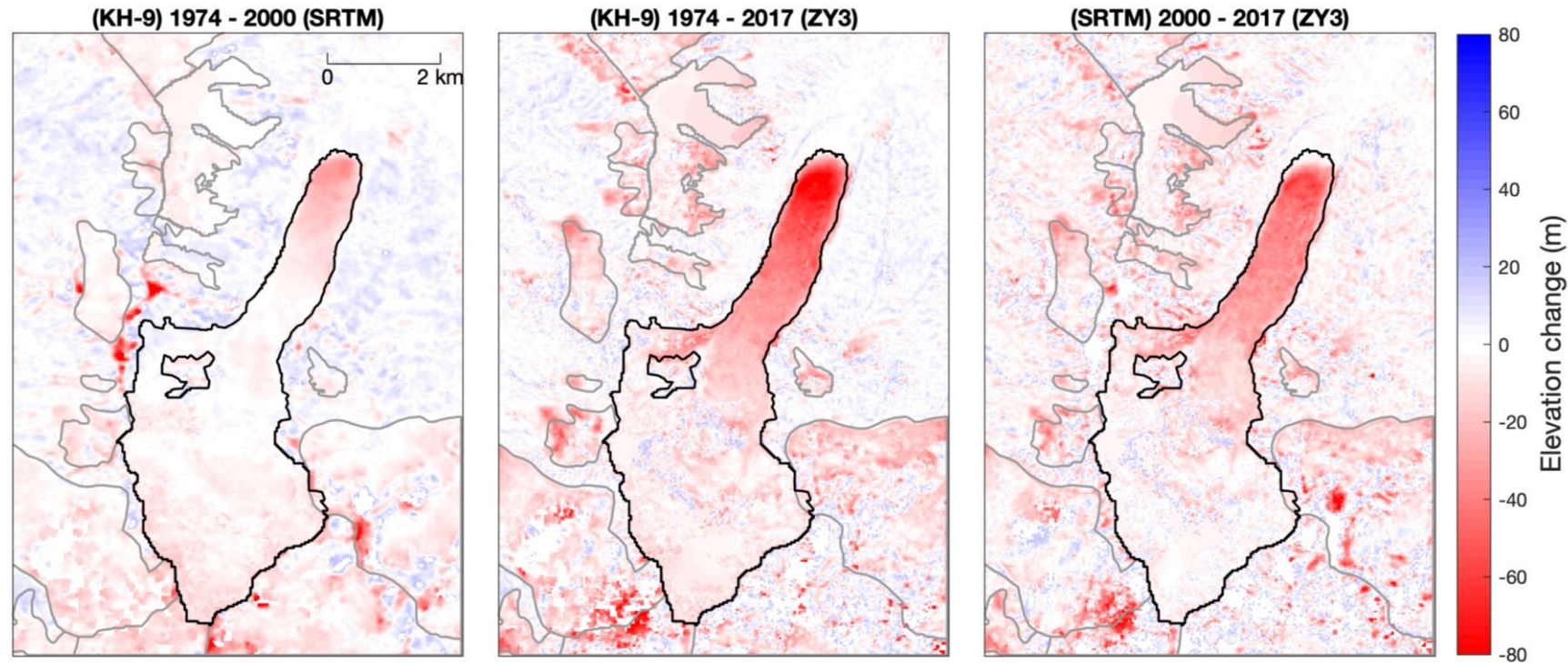
Forcing annual trends

Mean temperature and precipitation averaged over spring, monsoon and year-around at AWS_{off} location. The black-solid line is a 10-year moving average. The year repeated in the forcing experiment for each variable is shown in blue, selected as being the closest to the 1975-1989 average (blue line). The mean annual temperature trends computed over the period 1975-2018 ($+0.22^{\circ}\text{C}\cdot\text{dec}^{-1}$) and 1990-2018 ($0.39^{\circ}\text{C}\cdot\text{dec}^{-1}$) are shown in dashed lines blue and red respectively.



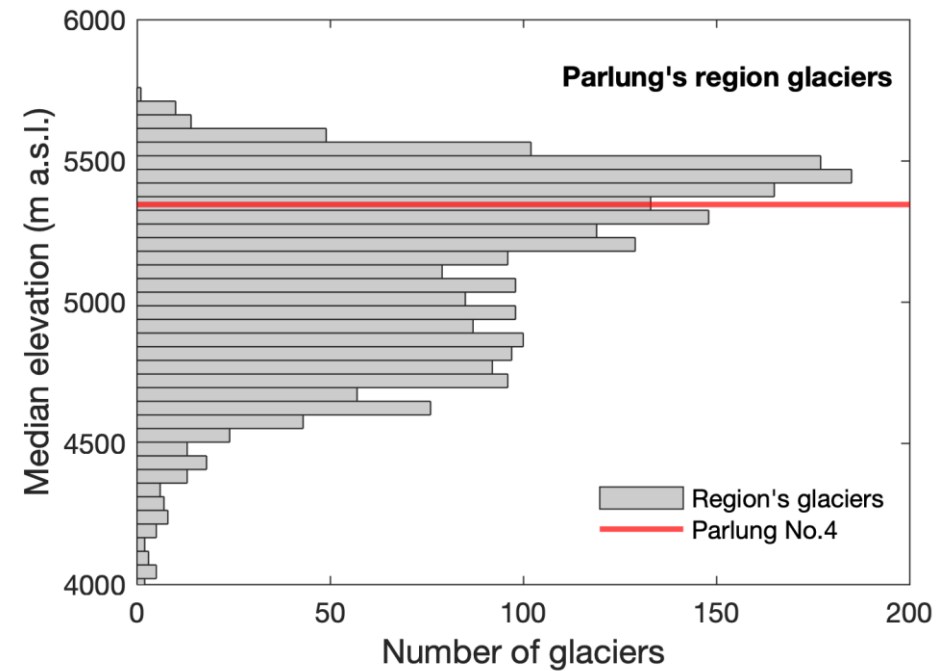
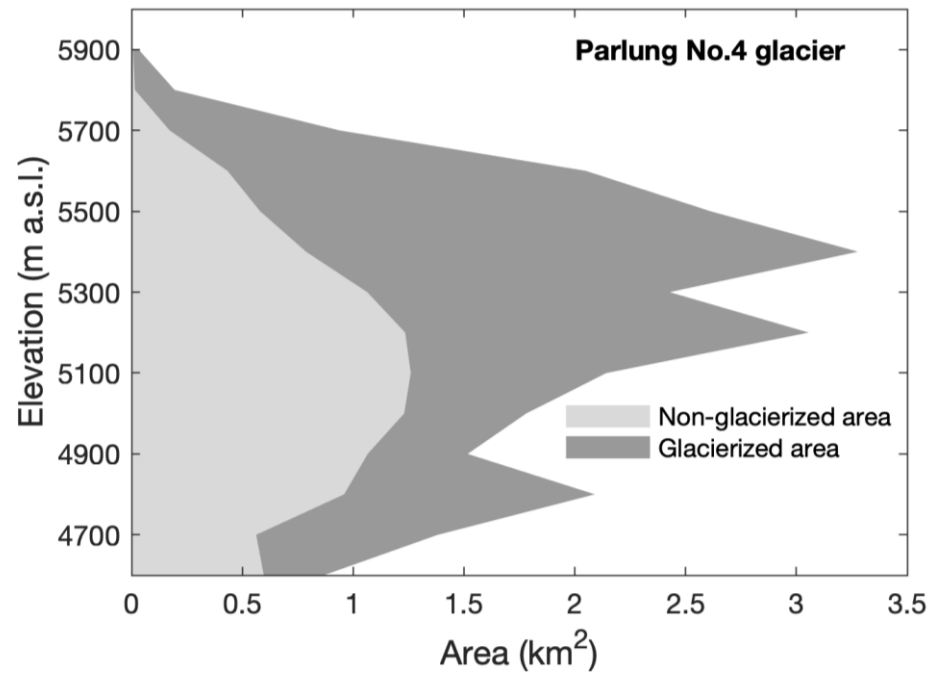
The red dots correspond to the year 2006, used as a detailed example of the experiment result (slide 30).

Remotely sensed surface elevation change



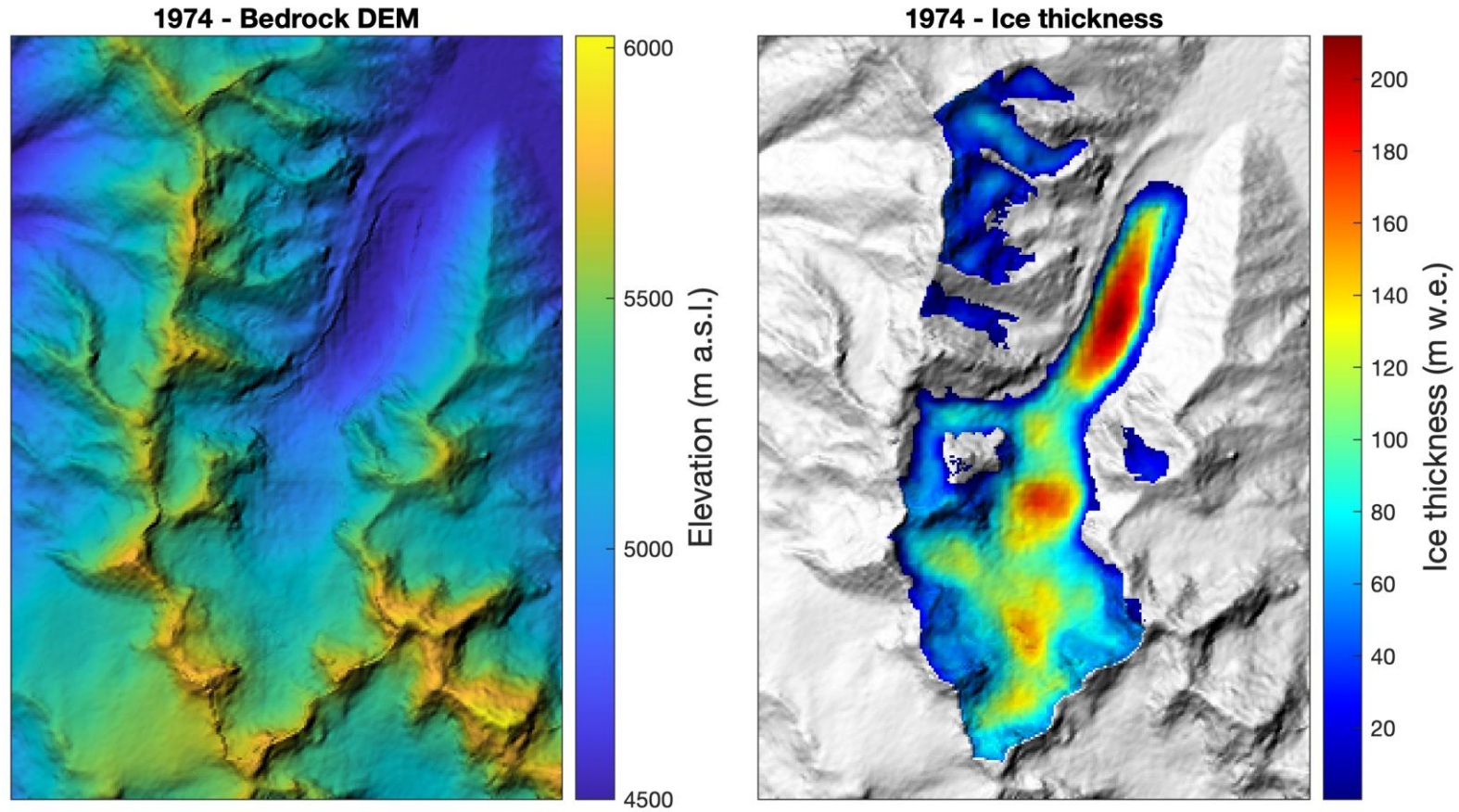
Elevation change maps derived from DEM differencing after the removing of outliers and gap-filling. No-data pixels are colored in black. The outlines of Parlung No.4 glacier are shown in black, and the outlines of the surrounding glaciers are shown in grey. The DEM of 1974 was derived from Hexagon KH-9 images by Dehecq et al. (2020)²⁵

Parlung No.4 hypsometry and representativeness



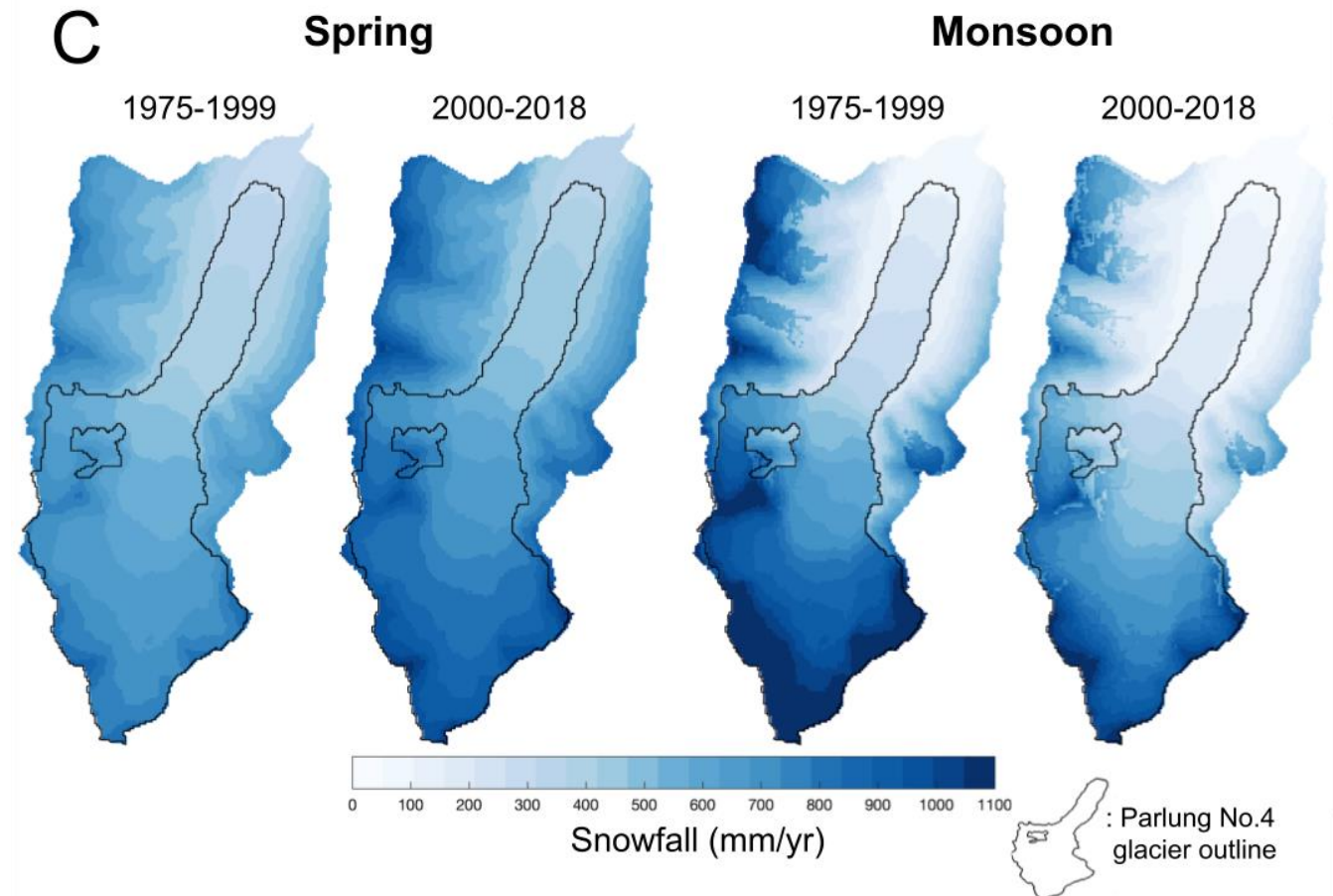
Median elevation distribution of glaciers in the proximity of Parlung No.4, the latter is highlighted in red

Parlung No.4 bedrock DEM and initial ice-thickness



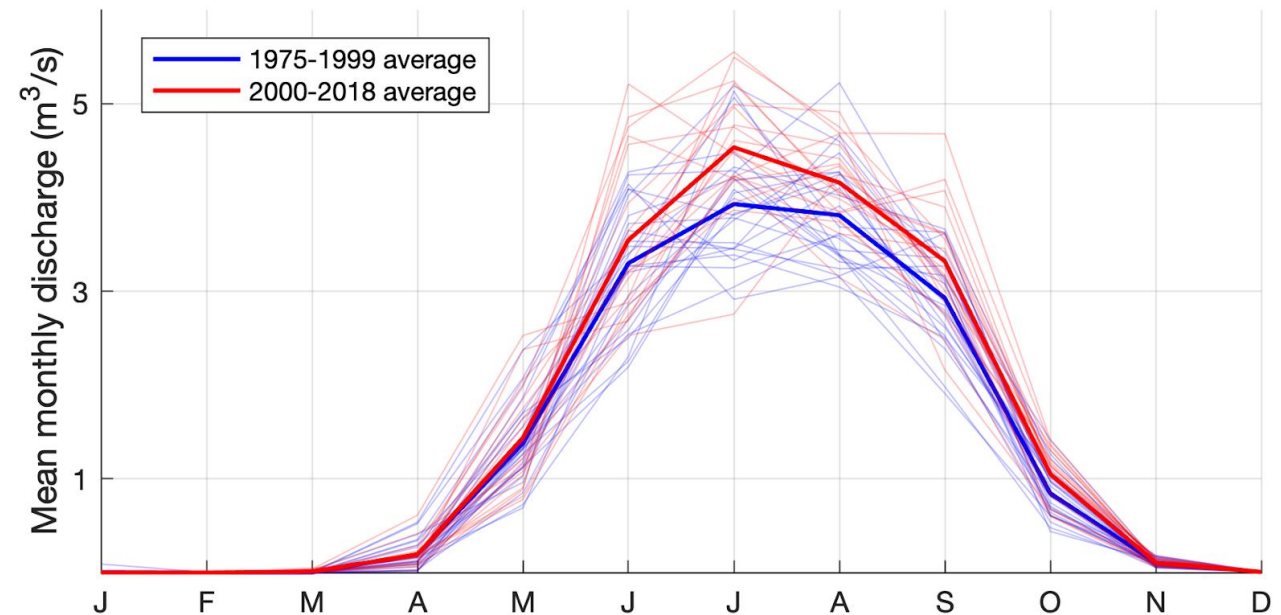
Spatial representation of spring and monsoon snowfall recent changes

- Increase in spring snowfall at all elevation
- Decrease in monsoon snowfall, especially pronounced in the high elevation areas
- Strong elevation gradient in monsoon snowfall due to both vertical precipitation and temperature gradient
- Less strong gradient in spring, since most of the catchment is below freezing temperature



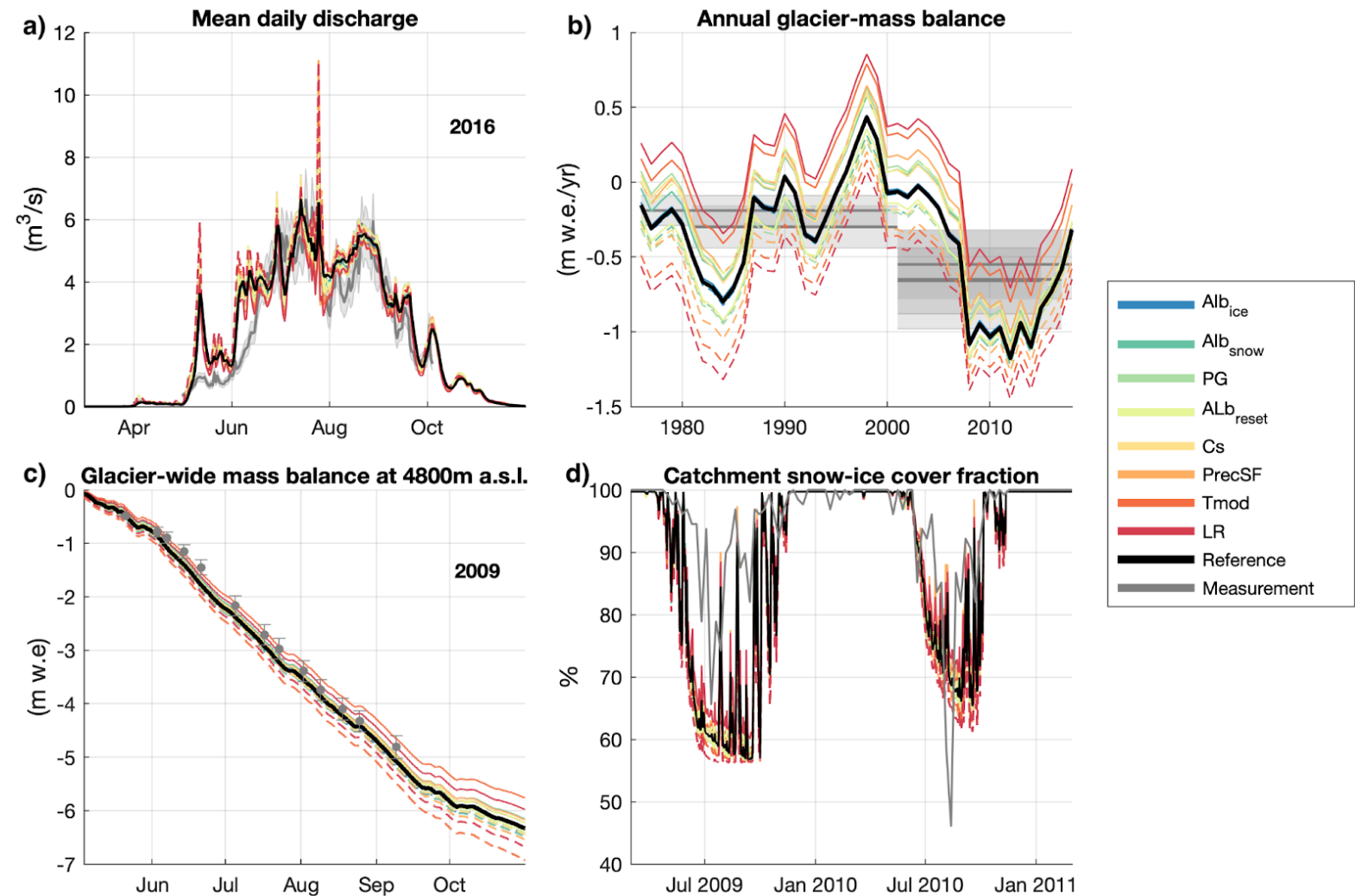
Monthly changes in catchment discharge

- No clear changes in catchment discharge before June
- Largest change are visible in June-July-August, and to a lesser extent in September
- No visible change in catchment discharge seasonality



Model performance sensitivity to parameters uncertainty

Sensitivity of the model performance against validation datasets to changes in the key model parameters. Each parameter was varied once at a time, within a plausible range. Dashed lines indicate a lower parameter value, while solid lines indicate a high parameter value. The results from the reference run and the values derived from observation are also shown as a basis for comparison.

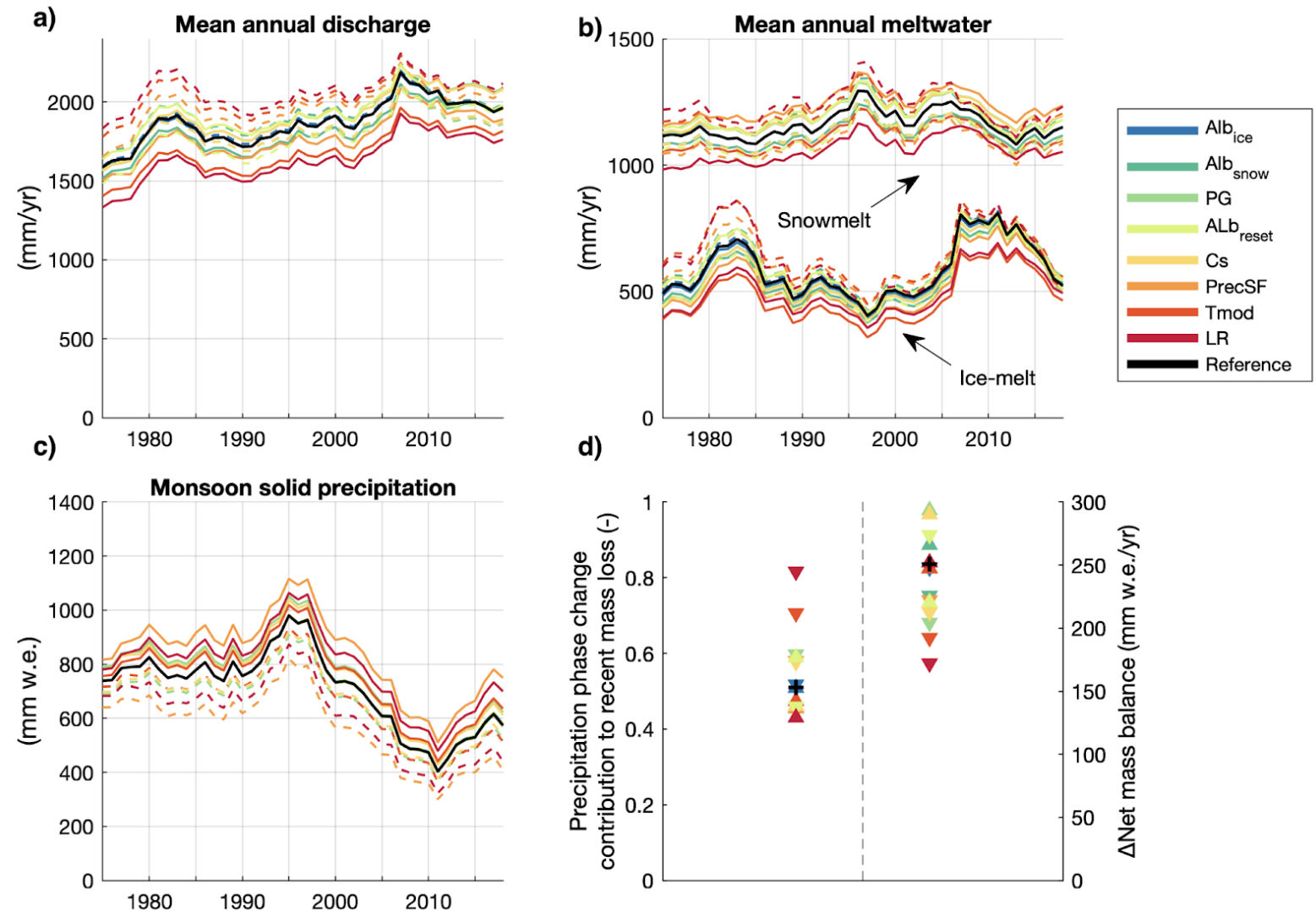


Results sensitivity to parameters uncertainty

Sensitivity of our main results to changes in the key model parameters. Each parameter was varied once at a time, within a plausible range. Dashed lines indicate a lower parameter value, while solid lines indicate a high parameter value. The results from the reference run (black line or black cross) are also shown as a basis for comparison. The Δ net mass balance corresponds to the change in mean annual solid water balance between the early (1975-1999) and the recent (2000-2018) period.

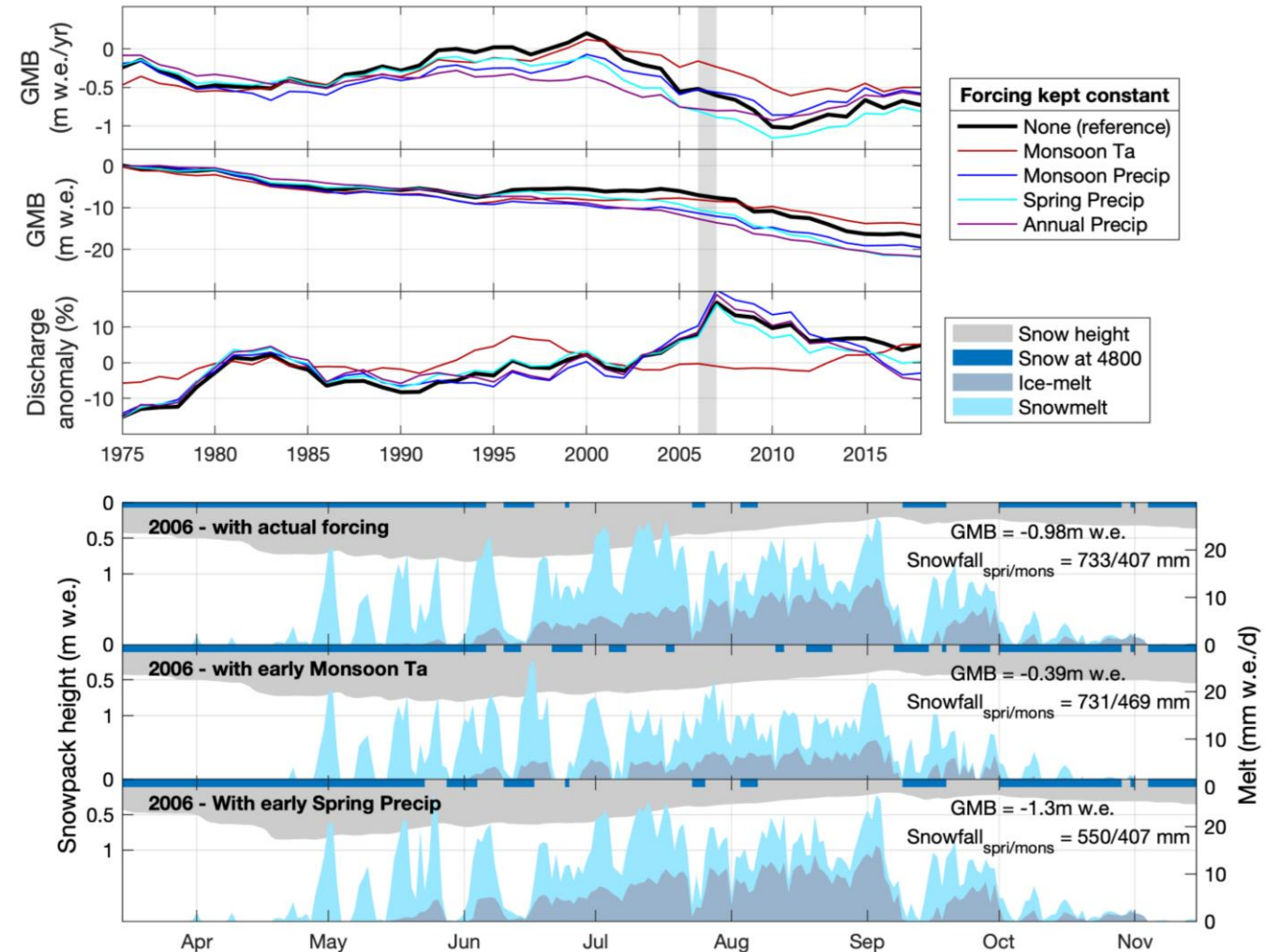


Our main results are not affected by the uncertainty in the parameters



Forcing experiment

- Aim : investigate the role of each meteorological variable in explaining the recent mass loss acceleration
- Variables of interest :
 - spring temperature
 - spring precipitation
 - monsoon temperature
 - monsoon precipitation
- Each variable was turn by turn artificially set to remain at its mean 1975-1985 level during the the whole simulation period



Forcing experiment

- When the monsoon temperature is set to the mean 1975-1985 conditions, the resulting annual GMB and catchment discharge during the recent period remained stable
- Similarly, higher spring and monsoon precipitation in 1995-2002 were responsible for the near-neutral GMB period
- Since 2005, increased spring precipitation and decreased monsoon precipitation have respectively mitigated and enhanced the mass loss primarily caused by monsoon warming

